Nanoscale

PAPER

View Article Online
View Journal | View Issue



Cite this: *Nanoscale*, 2023, **15**, 16612

# "*Setaria viridis*"-like cobalt complex derived Co/N-doped carbon nanotubes as efficient ORR/OER electrocatalysts for long-life rechargeable Zn–air batteries†

Shicheng Yi,‡ Rong Xin,‡ Xuxin Li, Yuying Sun, Mei Yang, Bei Liu, Hongbiao Chen, Huaming Li and Yijiang Liu *

The development of efficient and facile strategies to prepare metal and nitrogen codoped carbon (M–N–C) materials as oxygen electrocatalysts in rechargeable Zn–air batteries with high performance and a long life is challenging. Herein, we report a simple route to synthesize cobalt and nitrogen codoped carbon nanotubes (denoted as Co/N-CNT) as bifunctional oxygen electrocatalysts for rechargeable Zn–air batteries (ZABs). The Co/N-CNT are fabricated through the surface modification of carbon nanotubes with cobalt salt and melamine followed by pyrolysis, which delivers outstanding oxygen reduction/evolution reaction (ORR/OER) activity with a low overall potential gap ($\Delta E$ = 0.77 V) and remarkable durability. The home-made Zn–air batteries exhibit a high power density (130 mW $cm^{-2}$ *vs.* 82 mW $cm^{-2}$), a large specific capacity of (864 mA h $g^{-1}_{Zn}$ *vs.* 785 mA h $g^{-1}_{Zn}$), and a long cycling life (1200 h *vs.* 60 h) in both aqueous and solid media. This work opens an avenue for the reasonable surface modification of carbon nanotubes with various metals and heteroatoms to achieve high-performance electrocatalysts for clean and sustainable energy conversion and storage devices.

Received 13th July 2023,
Accepted 13th September 2023

DOI: 10.1039/d3nr03421f

rsc.li/nanoscale



## Introduction

The massive consumption of fossil fuels has aggravated the energy crisis and environmental pollution, thus triggering the development of green, clean and sustainable energy. Zn–air batteries (ZABs) have attracted tremendous attention in the field of renewable energy due to their high theoretical energy density, economy and safety.[1–3] Oxygen reduction/evolution reactions (ORR/OER) are elementary half-reactions that occur in the cathode of ZABs during discharge/charging processes, which are crucial to the cycling efficiency and durability of ZABs.[4,5] However, the sluggish ORR and OER kinetics have largely hindered the industrial application of ZABs owing to the complicated multi-electron transfer.[6,7] Noble metals, such as Pt- and Ir-based materials, are substantiated to be highly efficient catalysts to promote the reaction kinetics of ORR and OER, respectively, but their low abundance, high cost and insufficient stability are roadblocks for scalable applications.[8–10] Consequently, the exploitation of low cost bifunctional electrocatalysts with sufficient activity and long-term stability is vital to drive the applications of ZABs.

In the past few years, transition metal/N-doped carbon (M–N–C, M = Co, Ni, Fe, *etc.*) materials have attracted wide attention in electrocatalysis due to their comparable activity and superior durability to noble metal catalysts (*i.e.*, Pt/C).[11–15] The electrocatalytic activity of M–N–C is closely related to carbon scaffolds, such as the morphology (*i.e.*, sphere, sheet, tube, fiber, *etc.*) and structure (heteroatom-doping, graphitization, defects, *etc.*).[16,17] Among various carbon substrates, carbon nanotubes (CNT) stand out as promising supporting frameworks for oxygen electrocatalysts owing to their large surface area, high conductivity, good stability and mechanical flexibility.[18,19] Nonetheless, pristine carbon nanotubes show unfavorable inherent activity in ORR and OER because of the inactive $sp^2$ carbon atoms. The composition,[20,21] surface,[22] and defect engineering[23] methods are powerful ways to increase the electrocatalytic activity of CNT. For example, cobalt nanoparticle encapsulated nitrogen-doped carbon nanotubes (Co@N-CNTs) were obtained *via* the pyrolysis of a mixture of the cobalt substituted perfluorosulfonic acid/polytetrafluoroethylene copolymer and dicyandiamide, which

*College of Chemistry, Key Laboratory of Polymeric Materials & Application Technology of Hunan Province, Key Laboratory of Advanced Functional Polymeric Materials of College of Hunan Province, and Key Lab of Environment-Friendly Chemistry and Application in Ministry of Education, Xiangtan University, Xiangtan 411105, Hunan Province, P. R. China. E-mail: liuyijiang84@xtu.edu.cn*

†Electronic supplementary information (ESI) available. See DOI: https://doi.org/10.1039/d3nr03421f

‡These authors contributed equally to this work.

showed a high half-wave potential ($E_{1/2}$) of 0.805 V and excellent ORR stability.[24] $Co_3O_4$ decorated multi-walled carbon nanotubes (MWCNTs) synthesized by the supercritical fluid assisted method exhibited increased ORR activity due to their heterogeneous structure.[25] Notably, the combination of metal and heteroatom codoping can significantly promote the ORR/OER bifunctional electrocatalytic activity of CNT, while they are *in situ* formed during the pyrolysis of various precursor mixtures. The surface modification (*i.e.*, pre-modification) of carbon nanotubes is challenging due to the hydrophobic surface and aggregation of CNT.[26–28] Recently, E. Y. Choi and coworkers have developed Co nanoparticle encapsulated holey N-doped carbon nanotubes (Co@H-NCNTs) *via* two step pyrolysis, which exhibited low overpotentials for ORR and OER.[23] Although metal and heteroatom codoping can enhance the electrocatalytic activity of CNT, the rational surface modification of CNT to produce metal and heteroatom codoped bifunctional electrocatalysts with remarkable activity and durability for ZABs is still limited in scope.

Considering the above concerns, herein, we propose a facile, low-cost method to create Co nanoparticle encapsulated N-doped carbon nanotubes (abbreviated as Co/N-CNT) as prominent ORR/OER electrocatalysts for high performance and long life rechargeable ZABs. Specifically, $Co^{2+}$ is introduced into acid-treated CNT to give rise to Co-coordinated CNT followed by the addition of melamine, thereby forming *Setaria viridis*-like cobalt composites (Co-Mel-HMWCNT) *via* the coordination reactions. Subsequently, Co/N-CNT are obtained by carbonization of Co-Mel-HMWCNT composites at 800 °C. The influence of the $Co^{2+}$ content on the morphology of Co-Mel-HMWCNT composites and the resulting Co/N-CNT is investigated. Benefiting from the multi-active species and the special 1D architecture, the as-synthesized Co/N-CNT show prominent ORR ($J$ = 5.47 mA $cm^{-2}$, $E_{1/2}$ = 0.85 V) and OER ($E_{j=10}$ = 390 mV) catalytic activities with an overall oxygen potential difference ($\Delta E = E_{j=10} - E_{1/2}$) of 0.77 V and outstanding stability in 0.1 M KOH solution. The assembled ZABs using Co/N-CNT as the air cathode display a high power density (130 mW $cm^{-2}$ *vs.* 82 mW $cm^{-2}$), a large specific capacity (864 mA h $g^{-1}_{Zn}$ *vs.* 785 mA h $g^{-1}_{Zn}$), and a long cycle life (1200 h *vs.* 60 h) in both liquid and solid electrolytes. The pre-modification strategy of CNT reported in this work will enable the scalable and facile preparation of CNT-based electrocatalysts with impressive activity and durability to be a more realistic possibility in the energy conversion and storage field.

**Yijiang Liu**

*Dr Yijiang Liu is now a professor in the College of Chemistry at Xiangtan University, China. She received her M.S. degree from Xiangtan University in 2009 and PhD from the Institute of Chemistry, Chinese Academy of Sciences in 2015. She was a visiting scholar at Georgia Institute of Technology from 2017 to 2018. Her research work focuses on the design and preparation of advanced functional materials: porous carbon materials for efficient and durable electrocatalysts in energy conversion and storage devices; the crafting of highly stable perovskite nanocrystals for optical and electronic devices; Janus materials for concurrent catalysis and emulsification.*

## Experimental section

### Synthesis of Co-Mel-HMWCNT

A mixture of $H_2SO_4$ (98%) and $HNO_3$ (65%) solution (3 : 1, v/v) was added to MWCNT (500 mg) under vigorous stirring at 90 °C for 1 h. The mixture was cooled down, diluted, washed and dried to get the acidified MWCNT (HMWCNT, *i.e.*, O-rich CNT). 0.06 g of HMWCNT was thoroughly dispersed in 30 mL of methanol to form solution A under continuous ultrasonication. Meanwhile, 0.225 g of $Co(NO_3)_2{\cdot}6H_2O$ was dissolved in 10 mL of methanol to get solution B, and 0.50 g of melamine was dissolved in 30 mL of methanol to form solution C. Subsequently, solution B was poured into solution A under stirring at 25 °C for 16 h to form Co-HMWCNT. Finally, solution C was added to the Co-HMWCNT mixture under vigorous stirring at 60 °C for 24 h, and Co-coordinated CNT composites (Co-Mel-HMWCNT) were obtained by rotary evaporation. By varying the content of $Co(NO_3)_2{\cdot}6H_2O$, Co-Mel-HMWCNT composites with different morphologies were obtained. When the amounts of $Co(NO_3)_2{\cdot}6H_2O$ were changed to 150 mg and 300 mg, the corresponding samples were denoted $Co_{.067}$-Mel-HMWCNT and $Co_{1.33}$-Mel-HMWCNT.

### Synthesis of Co/N-CNT

Briefly, the obtained Co-Mel-HMWCNT was placed on a quartz boat and calcined at 800 °C for 2 h at a ramping rate of 3 °C $min^{-1}$ under a $N_2$ atmosphere. The final product was denoted as Co/N-CNT. For comparison, the samples without the addition of melamine and $Co(NO_3)_2$ were prepared and carbonized under the same conditions, which were denoted as Co-CNT and N-CNT, respectively. The corresponding samples of $Co_{.067}$-Mel-HMWCNT and $Co_{1.33}$-Mel-HMWCNT after pyrolysis were denoted $Co_{0.67}$/N-CNT and $Co_{1.33}$/N-CNT.

## Results and discussion

The synthetic route to Co/N-CNT is illustrated in Scheme 1. First, the original MWCNT were treated with an acid to create an O-rich surface, which can coordinate with $Co^{2+}$ to obtain Co-coordinated MWCNT (Co-HMWCNT). With the subsequent addition of melamine (Mel) at 60 °C, *Setaria viridis*-like Co-Mel-HMWCNT composites are obtained owing to the coordination between $Co^{2+}$, HMWCNT and melamine. Co nano-

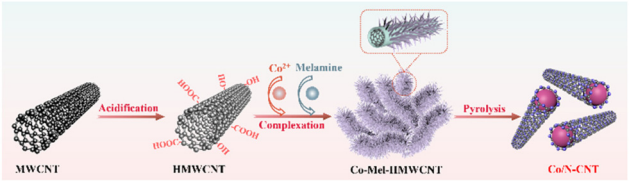


**Scheme 1** Schematic route to the Co/N-CNT electrocatalyst.

particle incorporated N-doped carbon nanotubes (Co/N-CNT) were obtained after pyrolysis of the Co-Mel-HMWCNT composites at 800 °C. For comparison, the samples of Co-CNT and N-CNT were prepared in parallel without the addition of melamine and Co salt, respectively. It is noteworthy that the content of Co salt can significantly affect the morphology of the Co-Mel-HMWCNT composites and the electrocatalytic activity of the resulting Co/N-CNT. MWCNT is curly and aggregated as shown in Fig. S1a,† while HMWCNT is more dispersive after acidifying (Fig. S1b†). With the addition of a low content of $Co(NO_3)_2$ (*i.e.*, $Co_{0.67}$), Co-HMWCNT can react with the partially dissolved melamine to form a Co-complex layer on CNT, thus interconnecting the CNT (Fig. S1c†). With the increase of Co content to $Co_{1.0}$ (*i.e.*, Co-Mel-HMWCNT), dense needle-like Co-melamine complexes are coated on and encapsulate CNT, forming *Setaria viridis*-like Co-Mel-HMWCNT composites (Fig. 1a). A further increase in the Co content to $Co_{1.33}$ can lead to short and big tube-like Co-melamine complex encapsulated CNT (Fig. S1d†). Co-Mel-HMWCNT composites with various $Co(NO_3)_2$ contents were carbonized and their electrocatalytic activity was scrutinized (Fig. S2†). The results indicate that $Co_{1.0}$/N-CNT (denoted as Co/N-CNT) obtained with a ratio of $Co^{2+}$ : melamine : HMWCNT of 225 : 500 : 60 exhibits the optimal electrocatalytic performance. Therefore, more detailed characterization of Co/N-CNT was performed in the following text.

The composition of Co-Mel-HMWCNT was characterized by FTIR, as depicted in Fig. S3.† The characteristic peak of carboxyl (–COOH) in HWMCNT at 1633 $cm^{-2}$ shifts to 1651 $cm^{-2}$, while the C=N peak of melamine at 1442 $cm^{-2}$ down-shifts to 1378 $cm^{-2}$, suggesting the interaction between $Co^{2+}$ and HMWCNT/melamine.[29,30] After pyrolysis of the Co-Mel-HMWCNT composites at 800 °C, Co nanoparticle encapsulated N-doped carbon nanotubes are observed (Fig. 1b). The TEM images show that Co/N-CNT is bamboo-like nanotubes, where Co nanoparticles (NPs) are wrapped by graphitic carbon layers (Fig. 1c). The interplanar spacing of Co NPs is 0.20 nm, corresponding to the Co (111) crystal plane (Fig. 1d).[31] The elemental mapping images of Co/N-CNT signify the presence of C, N, O, and Co, and the Co element is mainly concentrated on the tips of the CNTs (Fig. 1e).

The crystalline nature of Co/N-CNT was confirmed by X-ray diffraction (XRD) (Fig. 2a). The typical peaks that emerged at 75.85°, 51.52°, and 44.22° are assigned to the (220), (200), and (111) lattice planes of metal Co.[32] The graphitization degree of the Co/N-CNT was investigated by Raman spectroscopy (Fig. 2b). The two characteristic peaks at 1349 $cm^{-1}$ and 1588 $cm^{-1}$ match well with the D and G bands of Co/N-CNT.[33] Similar characteristic bands also emerge in the reference samples of Co-CNT and N-CNT. The proportions of the D band density to the G band density (*i.e.*, $I_D/I_G$) are 1.03, 1.14 and 1.30 for Co/N-CNT, Co-CNT and N-CNT, respectively. The lower $I_D/I_G$ value suggests the higher graphitization of Co/N-CNT, which is beneficial for the conductivity and thus the electrochemical performance of Co/N-CNT. The chemical composition and elemental valence of Co/N-CNT were further investigated by XPS measurement. The full XPS spectrum of Co/N-CNT reveals the presence of C, N, O, and Co elements (Fig. S4a†). The high-resolution N 1s spectrum of Co/N-CNT contains four species, *i.e.*, pyridinic-N (398.33 eV), Co–$N_x$

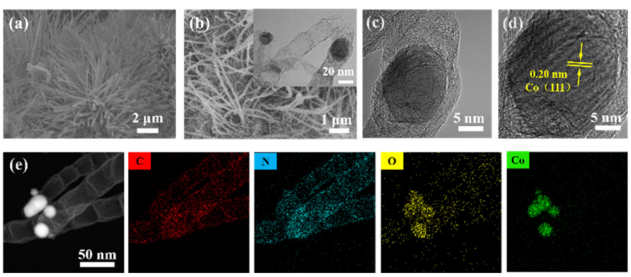


**Fig. 1** (a) SEM image of Co-Mel-HMWCNT composites; (b) SEM and inset TEM, (c) and (d) HRTEM, and (e) elemental mapping images of Co/N-CNT.

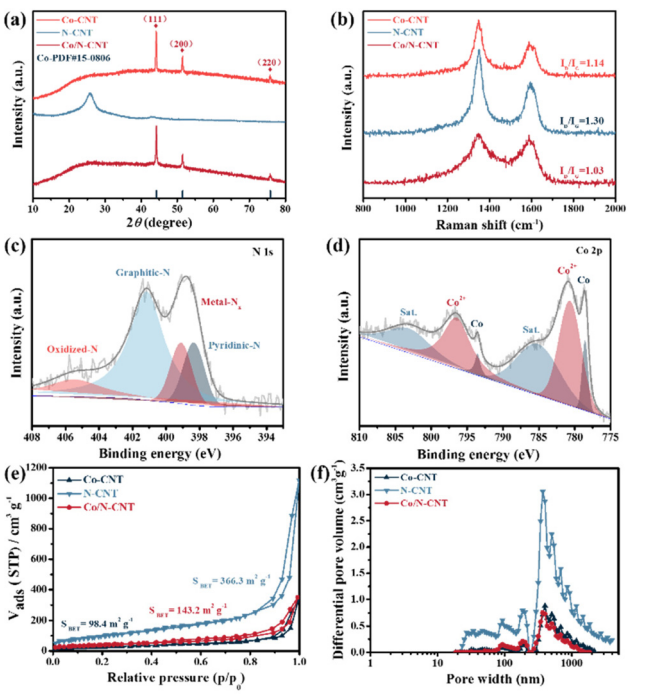


**Fig. 2** (a) XRD patterns, and (b) Raman analysis of Co/N-CNT, Co-CNT and N-CNT; high-resolution XPS analysis of (c) N 1s and (d) Co 2p of Co/N-CNT; (e) $N_2$ adsorption/desorption curves, and (f) the pore size distribution of Co/N-CNT, Co-CNT and N-CNT.

(399.09 eV), graphitic-N (401.15 eV) and oxidized-N (405.44 eV) (Fig. 2c).[34] The pyridinic-N and Co–$N_x$ are desirable active sites to boost ORR/OER activity.[35] The deconvoluted Co 2p spectrum of Co/N-CNT demonstrates the presence of $Co^0$ (778.52 and 793.51 eV), $Co^{2+}$ (780.63 and 796.43 eV), as well as satellite peaks located at 785.06 eV and 803.10 eV (Fig. 2d).[36] As shown in Fig. S4b,† the high-resolution C 1s spectrum of Co/N-CNT is deconvoluted into C–C (284.77 eV), C–N (285.95 eV), C–O (286.68 eV), and C=O (289.74 eV).[37] The O 1s can be mainly fitted into C=O (530.66 eV), C–O (531.71 eV), and H-OH (533.21 eV) (Fig. S4c†).[29] In addition, the porous structure (*i.e.*, surface area, pore size) of Co/N-CNT was examined by $N_2$ adsorption/desorption measurements. As depicted in Fig. 2e, the Co/N-CNT and the reference Co-CNT and N-CNT display type-IV isotherms with obvious hysteresis loops, suggesting the coexistence of mesopores and macropores. The specific surface areas of Co/N-CNT, Co-CNT, and N-CNT are 143.2 $m^2$ $g^{-1}$, 98.4 $m^2$ $g^{-1}$, and 366.3 $m^2$ $g^{-1}$, respectively. The pore sizes of Co/N-CNT and Co-CNT are smaller than that of N-CNT due to the incorporation of Co NPs, possibly plugging carbon nanotubes (Fig. 2f).

The electrocatalytic performance of Co/N-CNT as well as the reference samples of Co-CNT and N-CNT and commercial 20% Pt/C in the alkaline electrolyte (*i.e.*, 0.1 M KOH) were investigated by linear sweep voltammetry (LSV) measurements. We first scrutinized the influence of pyrolysis temperature on the catalytic activity of the resulting materials. As plotted in Fig. S5,† the Co/N-CNT obtained under 800 °C exhibit the optimal ORR and OER electrocatalytic performance. Fig. 3a depicts the LSV curves of Co/N-CNT, Co-CNT, N-CNT and Pt/C at a certain rotation rate of 1600 rpm. Clearly, the Co/N-CNT catalyst shows the best catalytic activity with an onset potential ($E_{on}$) of 0.97 V, a half-wave potential ($E_{1/2}$) of 0.85 V and a limited current density ($J$) of 5.47 mA $cm^{-2}$, much better than those of the Pt/C catalyst ($E_{on}$ = 0.96 V, $E_{1/2}$ = 0.84 V, $J$ = 5.16 mA $cm^{-2}$). Comparatively, the reference Co-CNT ($E_{1/2}$ = 0.79 V) and N-CNT ($E_{1/2}$ = 0.84 V) display inferior catalytic activity during the ORR in the absence of active N and Co species. In other words, Co and N codoping in Co/N-CNT provides sufficient active sites (pyridine-N, Co–$N_x$, *etc.*) to effectively improve the catalytic activity. Fig. 3b depicts the Tafel slopes of the as-synthesized catalysts. The Tafel slope of Co/N-CNT is 72 mV $dec^{-1}$, lower than that of Pt/C (75 mV $dec^{-1}$), Co-CNT (110 mV $dec^{-1}$), and N-CNT (97 mV $dec^{-1}$), indicating that the reaction kinetics of Co/N-CNT is much favourable. The ORR polarization curves of Co/N-CNT in the range of 400 to 2000 rpm are plotted in Fig. 3c, where the current density of Co/N-CNT increases linearly with increasing rotation speed, while $E_{on}$ remains unchanged. The average electron transfer number ($n$) of Co/N-CNT in the potential range of 0.3 V–0.7 V is 3.9 based on the Koutecky–Levich (K–L) equation (Fig. 3d), suggesting the primarily four-electron transfer process during ORR. Rotating ring disk electrode (RRDE) measurement was further employed to substantiate the four-electron transfer process. As shown in Fig. S6,† the number of transferred electrons determined from the RRDE data matches well with the

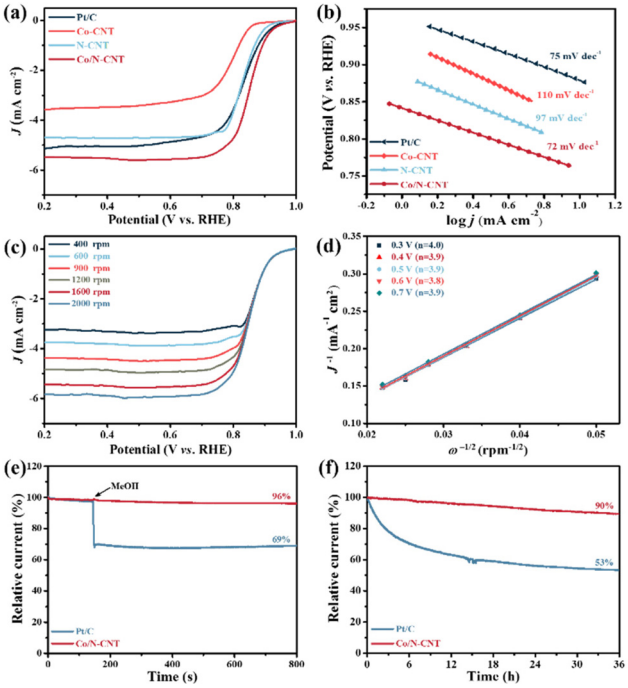


**Fig. 3** ORR performance of the as-crafted samples (*i.e.*, Co/N-CNT, Co-CNT, N-CNT and Pt/C) in 0.1 M KOH solution saturated with $O_2$: (a) LSV curves, (b) Tafel slopes, (c) LSV plots of Co/N-CNT at various speeds, (d) Koutecky–Levich plots of Co/N-CNT at different voltages, (e) methanol resistance, and (f) the chronoamperometry $i$–$t$ curves.

K–L plots, and the $HO_2^-$ yield is low (<7%). To illustrate the practical application, the methanol resistance and stability of Co/N-CNT in 0.1 M KOH were examined by chronoamperometric measurement ($i$–$t$). As shown in Fig. 3e, upon adding methanol to the electrolyte, Co/N-CNT show a negligible current loss, strikingly in contrast to the significant current decrease of Pt/C, representing the excellent methanol resistance of Co/N-CNT. The stability of Co/N-CNT during ORR is plotted in Fig. 3f, where the current retention is 90% after 36 h continuous testing. However, the current directly decreases to 53% for Pt/C under the same conditions. Therefore, the stability of Co/N-CNT is superior to Pt/C, benefiting the discharging behaviour of Co/N-CNT based Zn–air batteries.

The OER catalytic performance of Co/N-CNT was then investigated in a typical three-electrode device using 0.1 M KOH as the electrolyte. Fig. 4a shows the LSV curves of the tested materials, where the Co/N-CNT show the lowest $E_{on}$ and overpotential at 10 mA $cm^{-2}$ ($E_{j=10}$). The $E_{j=10}$ value of Co/N-CNT is 390 mV, which is smaller than Co-CNT (420 mV), N-CNT (510 mV), and comparable to $IrO_2$ (390 mV) (Fig. 4b). As shown in Fig. 4c, the Tafel slope of Co/N-CNT is 78 mV $dec^{-1}$, however, the Tafel slopes of $IrO_2$, Co-CNT, and N-CNT are 84 mV $dec^{-1}$, 90 mV $dec^{-1}$, and 126 mV $dec^{-1}$, respectively. The small Tafel slope of Co/N-CNT indicates the rapid OER kinetics and, thus, promising performance. Electrochemical impedance spectroscopy (EIS) was conducted to further illustrate the possible mechanism for the superior performance of

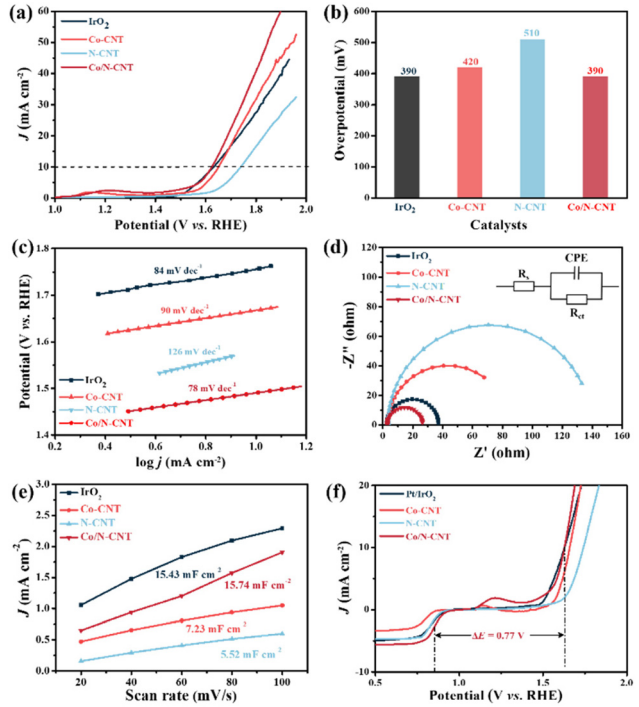


**Fig. 4** OER performance of the as-crafted samples (*i.e.*, Co/N-CNT, Co-CNT, N-CNT and $IrO_2$) in 0.1 M KOH solution saturated with $O_2$: (a) LSV curves, (b) OER overpotential at 10 mA $cm^{-2}$, (c) Tafel slopes, (d) Nyquist plots, (e) $C_{dl}$ values, and (f) integrated ORR/OER LSV curves.

Co/N-CNT. As shown in Fig. 4d, Co/N-CNT show the minimum semicircle with a charge transfer resistance ($R_{ct}$) of 27.10 Ω, while the $R_{ct}$ of Co-CNT and N-CNT are 70.60 and 135.5 Ω, respectively. The small $R_{ct}$ signifies the superior conductivity and the better electron transfer capability of Co/N-CNT over the reference samples.[38,39] The dual layer capacitance ($C_{dl}$) of Co/N-CNT, Co-CNT, N-CNT, and the benchmark $IrO_2$ were further determined by CV testing (Fig. S7†). As shown in Fig. 4e, the $C_{dl}$ value of Co/N-CNT is 15.74 mF $cm^{-2}$, significantly larger than Co-CNT (7.23 mF $cm^{-2}$), and N-CNT (5.52 mF $cm^{-2}$), demonstrating a higher electrochemically active surface area (ECSA) and sufficiently accessible active spaces during oxygen electrocatalysis.[40] The outstanding catalytic performance of Co/N-CNT may be attributed to the cooperation effect of various active species (*i.e.*, Co–$N_x$, pyridinic-N, Co NPs, *etc.*), unique 1D nanotube structure together with the relatively large surface area.

The long-time stability of the Co/N-CNT was recorded by the amperometric *i–t* test as shown in Fig. S8.† After continuous working for 30 h, the current density of Co/N-CNT was maintained at 87%, but that of $IrO_2$ decreased to only 66%, implying the remarkable OER durability of Co/N-CNT. The outstanding stability of Co/N-CNT was verified by TEM and XRD measurements after the OER stability testing. As shown in Fig. S9,† no noticeable morphological and crystalline structure variations are visualized after stability testing. Additionally, XPS analysis was conducted to further unveil the composition of Co/N-CNT after OER stability testing. As shown in Fig. S10a,† the emerging F element in the full survey spectrum is plausibly caused by the additives during the preparation of the cathode. The high-resolution Co 2p XPS spectrum after OER stability testing demonstrates that the $Co^{2+}$ peaks shift to higher binding energy and $Co^0$ peaks disappear, indicating partial surface oxidation of Co/N-CNT (Fig. S10b†). Generally, the overall potential gap between $E_{j=10}$ and $E_{1/2}$ ($\Delta E = E_{j=10} - E_{1/2}$) is a crucial indicator to represent the ORR/OER bifunctional performance of the electrocatalyst, and a low $\Delta E$ implies high electrocatalytic activity. As shown in Fig. 4f, the $\Delta E$ value of the Co/N-CNT electrocatalyst is 0.77 V, much lower than the reference Co-CNT ($\Delta E$ = 0.86 V) and N-CNT ($\Delta E$ = 0.90 V), and even competitive with Pt/$IrO_2$ (*i.e.*, assembled with Pt/C and $IrO_2$, 0.78 V) counterparts. Table S1† shows a comparison of Co NPs or Co single atom (SA) containing electrocatalysts in previous reports with this work, and the Co/N-CNT is comparable to and even better than most reported results.

The application of Co/N-CNT as the air-cathode catalyst in rechargeable ZABs for both liquid and solid electrolytes were studied, and Pt/$IrO_2$-based ZABs were also assembled simultaneously under the same conditions. As shown in Fig. 5a, the Co/N-CNT loaded air cathode is assembled with a zinc plate anode in 6 M KOH + 0.2 M $Zn(OAc)_2$. The open-circuit voltage of Co/N-CNT-based ZABs is 1.54 V, higher than that of Pt/$IrO_2$-based ZABs (1.43 V). The maximum power densities of Co/N-CNT and Pt/$IrO_2$-based ZABs are 130 mW $cm^{-2}$ and 112 mW $cm^{-2}$, respectively (Fig. 5b). Fig. 5c illustrates the excellent rate

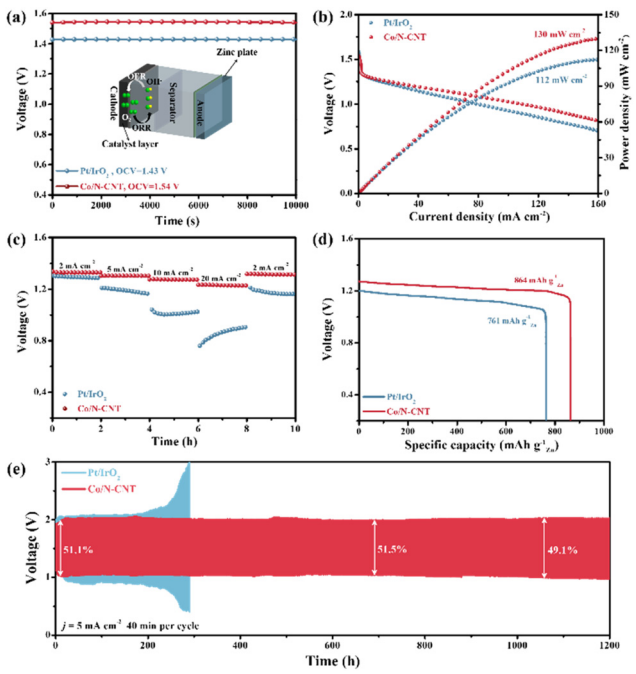


**Fig. 5** Performance of Co/N-CNT-assembled liquid ZABs: (a) open-circuit voltage plots (inset: schematic illustration of the assembled device), (b) polarization and power density curves, (c) galvanostatic discharge plots at different current densities, and (d) specific capacity at 5 mA $cm^{-2}$, and (e) discharge/charge cycling plots of Co/N-CNT and Pt/$IrO_2$.

performance of Co/N-CNT-based ZABs over Pt/$IrO_2$-based ZABs during galvanostatic discharging, where Co/N-CNT deliver a slight voltage loss in the current density range of 2–20 mA $cm^{-2}$. The potential can nearly recover to the initial value when the current density is back to 2 mA $cm^{-2}$. The specific capacities of Co/N-CNT and Pt/$IrO_2$-based ZABs are 864 mA h $g^{-1}_{Zn}$ and 761 mA h $g^{-1}_{Zn}$ at 5 mA $cm^{-2}$ (Fig. 5d), respectively. The charging/discharging cycling stability of Co/N-CNT and Pt/$IrO_2$-based ZABs is measured at 5 mA $cm^{-2}$ with 20 min discharging and 20 min charging per cycle. As shown in Fig. 5e, the original voltage gap and energy efficiency of Co/N-CNT-based ZABs are 0.95 V and 51.1%. A small voltage gap increase and a slight energy efficiency drop are found after unremitting working for 1200 h (*i.e.*, 1800 discharging/charging cycles). In striking contrast, Pt/$IrO_2$-based ZABs can only operate for 200 h. The outstanding performance of the Co/N-CNT-made liquid ZABs is competitive with the reported literature as summarized in Table S2.†

In addition, the use of Co/N-CNT in flexible ZABs was investigated. The Co/N-CNT, zinc plate, and self-prepared sodium polyacrylate (PANa) gel were combined in a two-electrode configuration, and the Pt/$IrO_2$-based counterpart was also made in parallel (inset of Fig. 6a). The open-circuit voltage and maximum power density of Co/N-CNT and Pt/$IrO_2$-based flexible ZABs are 1.44 V/1.40 V (Fig. 6a), and 82 mW $cm^{-2}$/28 mW $cm^{-2}$ (Fig. 6b), respectively. The Co/N-CNT displays excellent galvanostatic discharging ability from 1 mA $cm^{-2}$ to 4 mA $cm^{-2}$ with a negligible voltage drop. Notably, the potential can be fully recovered when a current density of 1 mA $cm^{-2}$ is applied, demonstrating the impressive rate performance (Fig. 6c). The specific capacities of Co/N-CNT and Pt/$IrO_2$-based flexible ZABs are determined to be 785 mA h $g^{-1}_{Zn}$ and 735 mA h $g^{-1}_{Zn}$ at 2 mA $cm^{-2}$ (Fig. 6d), respectively. The cycling stability of the assembled flexible ZABs is recorded at 20 min per cycle as shown in Fig. 6e. It can be seen that the Co/N-CNT-based flexible ZAB can stably work for 60 h at 2 mA $cm^{-2}$, in sharp contrast to 15 h of the Pt/$IrO_2$ counterparts. Such remarkable ZAB performance of Co/N-CNT is highly dependent on its prominent ORR/OER bifunctional activity and durability in alkaline medium.

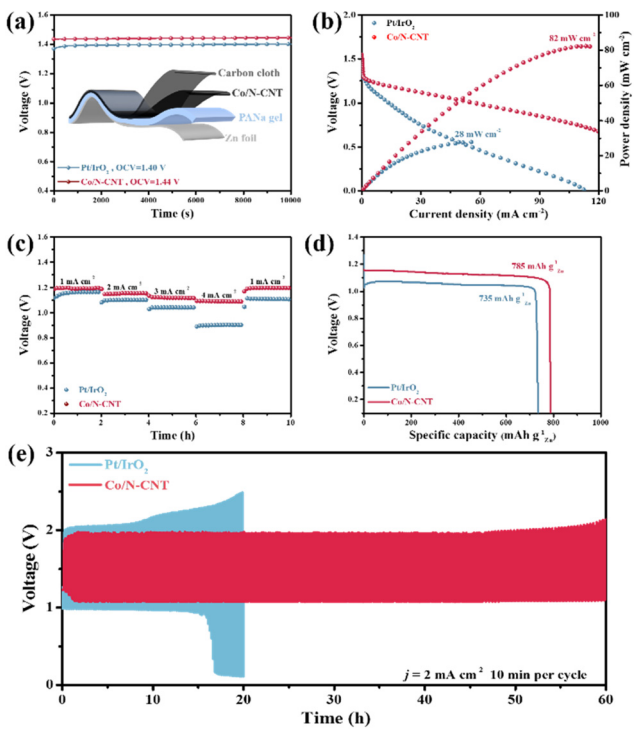


**Fig. 6** Performance of the home-made Co/N-CNT-based flexible ZABs: (a) open-circuit voltage plots (inset: schematic illustration of the flexible devices), (b) polarization and power density curves, (c) galvanostatic discharge plots at different current densities, and (d) specific capacity measured at a current density of 2 mA $cm^{-2}$, (e) galvanostatic discharge/charge cycling of Co/N-CNT and Pt/$IrO_2$.

## Conclusions

In summary, we have proposed an effective method to construct cobalt NP embedded nitrogen-doped carbon nanotubes (Co/N-CNT) as bifunctional electrocatalysts with excellent activity and stability for both ORR and OER in alkaline electrolytes. *Setaria viridis*-like Co-Mel-HMWCNT composites were first synthesized by the interaction between $Co^{2+}$, melamine and WMCNT at a suitable ratio. The pyrolysis of Co-Mel-HMWCNT composites at the optimal temperature yielded Co/N-CNT with a bamboo-like nanotube architecture, a large surface area, and well-distributed Co NPs. The as-crafted Co/N-CNT exhibited high ORR/OER catalytic activity with an $E_{1/2}$ of 0.85 V and an $E_{j=10}$ of 390 mV, and the reversible oxygen electrode index of 0.77 V. The Co/N-CNT-based ZAB in the liquid electrolyte delivered a high specific capacity (864 mA h $g^{-1}_{Zn}$ at 5 mA $cm^{-2}$), power density (130 mW $cm^{-2}$), and remarkable cycling stability (1800 cycles over 1200 h at 5 mA $cm^{-2}$). Most importantly, the assembled flexible ZAB also demonstrated remarkable performance and outstanding cycling stability (60 h at 2 mA $cm^{-2}$). The strategy for the fabrication of Co/N-CNT may provide a promising way for the functionalization of CNT for energy storage and conversion devices.

## Author contributions

Shicheng Yi: investigation, data analysis, validation, and writing – original draft. Rong Xin: investigation, data analysis, validation, and writing – revision. Xuxin Li: data analysis and validation. Yuying Sun: data analysis and validation. Mei Yang: data analysis and validation. Bei Liu: data analysis and validation. Hongbiao Chen: data analysis and validation. Huaming Li: data analysis and validation. Yijiang Liu: supervision, methodology, data analysis, validation, writing – review & editing, and funding acquisition.

## Conflicts of interest

There are no conflicts to declare.

## Acknowledgements

This work was supported by the National Natural Science Foundation of China (52173207), the Science Fund for Distinguished Young Scholars of Hunan Province of China (2023JJ10040), the Science and Technology Innovation Program of Hunan Province (2022RC1077), and the Outstanding Youth Fund Project of Hunan Provincial Department of Education (21B0119).

## References

1 C. G. Hu, R. Paul, Q. B. Dai and L. M. Dai, *Chem. Soc. Rev.*, 2021, **50**, 11785–11843.
2 T. P. Zhou, N. Zhang, C. Z. Wu and Y. Xie, *Energy Environ. Sci.*, 2020, **13**, 1132–1153.
3 X. X. Shu, M. M. Yang, D. X. Tan, K. S. Hui, K. N. Hui and J. T. Zhang, *Mater. Adv.*, 2021, **2**, 96–114.
4 H. W. Chen, Y. J. Liu, B. Liu, M. Yang, H. M. Li and H. B. Chen, *Nanoscale*, 2022, **14**, 12431–12436.
5 L. Yan, B. B. Xie, C. Yang, Y. H. Wang, J. Q. Ning, Y. J. Zhong and Y. Hu, *Adv. Energy Mater.*, 2023, **13**, 2204245.
6 Y. G. Zhao, D. P. A. Saseendran, C. Huang, C. A. Triana, W. R. Marks, H. Chen, H. Zhao and G. R. Patzke, *Chem. Rev.*, 2023, **123**, 6257–6358.
7 Y. M. Liu, J. H. Ma, T. K. A. Hoang, L. J. Yang and Z. H. Chen, *Nanoscale*, 2023, **15**, 1172–1179.
8 J. J. Ban, H. J. Xu, G. Q. Cao, Y. M. Fan, W. K. Pang, G. S. Shao and J. H. Hu, *Adv. Funct. Mater.*, 2023, **33**, 2300623.
9 S. C. Cai, Z. H. Meng, G. J. Li, Y. An, Y. P. Cheng, E. J. Kan, B. O. Yang, H. N. Zhang and H. L. Tang, *Nano Res.*, 2023, **16**, 5887–5893.
10 W. W. Xie, T. Z. Tian, M. Yang, N. W. Li and L. Yu, *Appl. Catal., B*, 2022, **317**, 121760.
11 C. X. Zhao, J. N. Liu, J. Wang, D. Ren, B. Q. Li and Q. Zhang, *Chem. Soc. Rev.*, 2021, **50**, 7745–7778.
12 F. J. Guo, M. Y. Zhang, S. C. Yi, X. X. Li, R. Xin, M. Yang, B. Liu, H. B. Chen, H. M. Li and Y. J. Liu, *Nano Res. Energy*, 2022, **1**, e9120027.
13 T. Wang, Y. He, Y. J. Liu, F. J. Guo, X. F. Li, H. B. Chen, H. M. Li and Z. Q. Lin, *Nano Energy*, 2021, **79**, 105487–105497.
14 T. T. Qin, J. Q. Niu, X. Q. Liu, C. Y. Geng and A. P. O'Mullane, *ACS Appl. Mater. Interfaces*, 2023, **15**, 7987–7998.
15 S. G. Wang, J. W. Qing, T. Meng and M. H. Cao, *Nano Energy*, 2017, **39**, 626–638.
16 C. Jin, H. J. Deng, J. Zhang, Y. Hao and J. J. Liu, *Chem. Eng. J.*, 2022, **434**, 134617.
17 M. Li, S. H. Chen, B. Li, Y. Q. Huang, X. W. Lv, P. P. Sun, L. Fang and X. H. Sun, *Electrochim. Acta*, 2021, **338**, 135857.
18 Q. X. Zhou, S. K. Zhang, G. Y. Zhou, H. Pang, M. Y. Zhang, L. Xu, K. Sun, Y. W. Tang and K. Huang, *Small*, 2023, 2301324.
19 C. Zhang, H. F. Dong, B. L. Chen, T. X. Jin, J. Nie and G. P. Ma, *Carbon*, 2021, **185**, 17–26.
20 A. Pendashteh, J. Palma, M. Anderson, J. J. Vilatela and R. Marcilla, *ACS Appl. Energy Mater.*, 2018, **1**, 2434–2439.
21 Y. Meng, Y. M. Zhao, J. C. Li, C. Shi, L. L. Zhang, P. X. Hou, C. Liu and H. M. Cheng, *NPG Asia Mater.*, 2023, **15**, 14.
22 B. Q. Li, S. Y. Zhang, B. Wang, Z. J. Xia, C. Tang and Q. Zhang, *Energy Environ. Sci.*, 2018, **11**, 1723–1729.
23 E. Y. Choi, D. E. Kim, S. Y. Lee, C. B. Park and C. K. Kim, *Appl. Catal., B*, 2023, **325**, 122386.
24 H. H. Wu, X. L. Jiang, Y. F. Ye, C. C. Yan, S. H. Xie, S. Miao, G. X. Wang and X. H. Bao, *J. Energy Chem.*, 2017, **26**, 1181–1186.
25 P. Thangasamy, K. Selvakumar, M. Sathish, S. M. S. Kumar and R. Thangamuthu, *Catal. Sci. Technol.*, 2017, **7**, 1227–1234.
26 A. P. Grosvenor, M. C. Biesinger, R. S. C. Smart and N. S. McIntyre, *Surf. Sci.*, 2006, **600**, 1771–1779.
27 B. H. Zhang, M. Y. Wu, L. Zhang, Y. Xu, W. D. Hou, H. Z. Guo and L. Wang, *J. Colloid Interface Sci.*, 2023, **629**, 640–648.
28 Y. Liu, D. P. Ji, M. Li, J. Xiao, P. Dong, C. X. Zhang, L. N. Han and Y. J. Zhang, *J. Alloys Compd.*, 2020, **842**, 155791.
29 W. C. Xie, Y. J. Liu, Y. Yan, M. Yang, M. Y. Zhang, B. Liu, H. M. Li, H. B. Chen and Z. Q. Lin, *Energy Storage Mater.*, 2023, **59**, 102783–102793.
30 X. F. Li, Y. J. Liu, H. B. Chen, M. Yang, D. G. Yang, H. M. Li and Z. Q. Lin, *Nano Lett.*, 2021, **21**, 3098–3105.
31 G. D. Chen, Y. Y. Xu, L. Huang, A. I. Douka and B. Y. Xia, *J. Energy Chem.*, 2021, **55**, 183–189.
32 Q. R. Liang, H. H. Jin, Z. Wang, Y. L. Xiong, S. Yuan, X. C. Zeng, D. P. He and S. C. Mu, *Nano Energy*, 2019, **57**, 746–752.
33 F. Kong, X. Z. Cui, Y. F. Huang, H. L. Yao, Y. F. Chen, H. Tian, G. Meng, C. Chen, Z. W. Chang and J. L. Shi, *Angew. Chem., Int. Ed.*, 2022, **61**, e202116290.
34 H. W. Zhang, M. Q. Zhao, H. R. Liu, S. R. Shi, Z. H. Wang, B. Zhang, L. Song, J. Z. Shang, Y. Yang, C. Ma, L. R. Zheng, Y. H. Han and W. Huang, *Nano Lett.*, 2021, **21**, 2255–2264.
35 M. M. Fan, Q. X. Yuan, Y. Y. Zhao, Z. M. Wang, A. Wang, Y. Y. Liu, K. Sun, J. J. Wu, L. Wang and J. C. Jiang, *Adv. Mater.*, 2022, **34**, 2107040.
36 C. B. Sun, J. Ding, H. Z. Wang, J. Liu, X. P. Han, Y. D. Deng, C. Zhong and W. B. Hu, *J. Mater. Chem. A*, 2021, **9**, 13926–13935.
37 Z. K. Yang, C. M. Zhao, Y. T. Qu, H. Zhou, F. Y. Zhou, J. Wang, Y. E. Wu and Y. D. Li, *Adv. Mater.*, 2019, **31**, 1808043.
38 Z. Wang, J. M. Ang, J. Liu, X. Y. D. Ma, J. H. Kong, Y. F. Zhang, T. Yan and X. H. Lu, *Appl. Catal., B*, 2020, **263**, 118344.
39 C. H. Zhou, X. Chen, S. Liu, Y. Han, H. B. Meng, Q. Y. Jiang, S. M. Zhao, F. Wei, J. Sun, T. Tan and R. F. Zhan, *J. Am. Chem. Soc.*, 2022, **144**, 2694–2704.
40 H. Lv, Y. N. Zheng, Y. Z. Wang, J. L. Wang, B. Liu and Z. A. Qiao, *Angew. Chem., Int. Ed.*, 2023, **62**, e202304420.